CSIAM Trans. Appl. Math.
doi: 10.4208/csiam-am.SO-2023-0009

Vol. 7, No. 1, pp. 120-145
March 2026

A Hue-Preserving Color Image Restoration Model Using Saturation-Value Total Variation

Wei Wang* and Yuming Yang

School of Mathematical Sciences, Key Laboratory of Intelligent Computing and Applications (Ministry of Education), Tongji University, Shanghai 200092, China.

Received 6 March 2023; Accepted 28 April 2025

Abstract. In this paper, we propose and develop a novel hue-preserving color image restoration model. In the proposed model, saturation-value total variation is used as the regularization term. In order to reduce hue loss during regularization, the hue-preserving technique is incorporated into the proposed energy functional. We then rewrite the proposed model equivalently into a three-block separable convex version and apply an alternating direction method of multipliers based algorithm to solve the proposed equivalent model numerically. We also give the convergence analysis of the proposed algorithm. Numerical examples are presented to demonstrate that the performance of the proposed restoration model is better than that of other testing methods in terms of visual quality and some criteria such as peak signal-to-noise ratio, structure similarity, and spatial-CIELAB color error.

AMS subject classifications: 65K10, 68U10, 90C25

Key words: Color image restoration, hue-preserving, saturation-value total variation, alternating direction method of multipliers.

1 Introduction

Variational techniques have been successfully applied to color image processing. Total variation (TV) [18], originally used to solve the gray image restoration problems, was generalized to handle color images by using different versions of color total variation. Blomgren and Chan [2] proposed a color TV regularization with a global channel coupling by summing the variation of each channel. Bresson and Chan [4] considered local channel coupling and proposed another color TV (CTV) regularization with channel-coupled monotonic functions. Sapiro [19] studied spectral information of the tensor $(\nabla \mathbf{u})^\top \nabla \mathbf{u}$ where $\mathbf{u}(x,y)$ is a vector-valued image defined on the bounded image domain $\Omega \subset \mathbb{R}^2, \nabla$ is the gradient operator, and proposed a vectorial TV (VTV) model by intro-

*Corresponding author. *Email addresses:* wangw@tongji.edu.cn (W. Wang), yangym@tongji.edu.cn (Y. Yang)

ducing a penalty function on the eigenvalues of $(\nabla \mathbf{u})^\top \nabla \mathbf{u}$. Rodriguez and Wohlberg [17] used the iteratively reweighted norm approach to propose a simple and flexible method to handle the generalized VTV (GVTV) functional by replacing the l^q norm with the weighted l^2 norm. We remark here that all the above mentioned variational models are formulated based on RGB (red, green, blue) color space. Another useful color representation model is HSV (hue, saturation, value) color space which is similar to human color perception. Jia, Ng and Wang [11] proposed and developed a new saturation-value total variation (SV-TV) in HSV color space for color image restoration, which has two parts with different components: one is to minimize the gradient of the saturation, another one aims to control the smoothness of the image regions. SV-TV regularization guarantees a great reduction of unexpected chromatic intersection. However, minimization of the saturation difference will cause the loss of hue in practice.

Hue is one of the inherent attributes of a color which decides what kind of color it is. Therefore, preserving the hue unchanged is an important issue in color image processing. Yang and Rodriguez [22] proposed two hue-preserving techniques (affine transforms: scaling and shifting) to process luminance and saturation components. Naik and Murthy [14] used similar affine transforms to propose a scheme to generalize the grayscale image enhancement method to color image enhancement with hue preserved. Based on different hue-preserving technology, many color image enhancement methods have been proposed [1, 5, 10, 13]. Fitschen *et al.* [5] took advantage of the fact that affine transformations do not change hue and proposed a variational hue-preserving technique flexibly preserving hue by solving an optimization problem. The above hue-preserving technique has been used in [15, 16, 20] for color image enhancement. Hue-preserving techniques have been widely used in color image enhancement in the literature, however, rarely applied to color image restoration problems.

The main aim of this paper is to propose and develop a novel hue-preserving color image restoration model using SV-TV. In the proposed model, we make use of SV-TV as the regularization term, and we incorporate an efficient hue-preserving technique into the proposed energy functional in order to reduce hue loss during regularization. We then formulate the proposed energy function by combining the regularization term, the data-fitting term and the hue-preserving term. In order to solve the proposed minimization problem efficiently, we rewrite the proposed model equivalently into a three-block separable convex version. Numerically, we propose a very efficient and effective algorithm with convergence guaranteed to solve the proposed optimization problem. The alternating direction method of multipliers (ADMM) [3, 6, 7] is a benchmark algorithm for solving a linearly constrained convex minimization model with a two-block separable objective function. Many ADMM-based methods for multi-block convex programming have been studied in [8, 9]. In this paper, we apply an ADMM-based algorithm with convergence guaranteed to solve the proposed model. We give the convergence analysis of the proposed algorithm by using the similar arguments in [9] for a three-block ADMM algorithm. In summary, the contribution of this paper is as follows. First, we propose and develop a novel color image restoration model by using saturation-value total variation

for removing color artifacts and hue-preserving technique for keeping hue information. Second, we present a very efficient and effective algorithm based on ADMM to solve the proposed optimization problem. Finally, the existence of the solution of the proposed model and the convergence analysis of the proposed algorithm have been studied. Numerical examples are presented to demonstrate that the performance of the proposed restoration model is better than that of other testing methods in terms of visual quality and some criteria such as peak signal-to-noise ratio (PSNR), structure similarity (SSIM), and S-CIELAB color error [23].

The outline of this paper is given as follows. In Section 2, we will recall the related work. In Section 3, we will introduce the proposed hue-preserving color image restoration model using SV-TV. In Section 4, we will present the proposed numerical algorithm to solve the proposed optimization problem. In Section 5, we will report some numerical examples to demonstrate the effectiveness of the proposed model. Finally, some concluding remarks are given in Section 6.

2 Related work

Assume that $\mathbf{u}=[u_r,u_g,u_b]^\top:\Omega\to[0,1]^3$ is a color image, Ω is a connected bounded open subset of R^2 with compact Lipschitz boundary, and $(x,y)\in\Omega$ is the 2-D spatial location in the image domain.

2.1 Hue preservation

In this section, we recall the hue-preserving technique we will use in this paper. The following proposition illustrates this technique by showing the characteristics of the pixels with the same chromaticity, see [5] for details.

Proposition 2.1. *The single pixels $(r_0,g_0,b_0)\in[0,1]^3$ and $(r,g,b)\in[0,1]^3$ have the same hue if and only if there exist $a,d\in R$ such that $(r,g,b)=a(r_0,g_0,b_0)+d\mathbf{1}_3^\top$, where $\mathbf{1}_3:=(1,1,1)^\top$.*

In order to make the use of hue-preserving techniques flexible, a is expected to become a set of approximate numbers. Two auxiliary variables $\mathbf{v}=[v_1,v_2,v_3]^\top:\Omega\to[0,1]^3$ and $d:\Omega\to\mathbb{R}$ are introduced, so that the map between $\mathbf{u}$ and the reference image $\mathbf{h}=[h_r,h_g,h_b]^\top:\Omega\to[0,1]^3$ is established as

$$u_r=\frac{h_r}{h_0}v_1+d,\quad u_g=\frac{h_g}{h_0}v_2+d,\quad u_b=\frac{h_b}{h_0}v_3+d,$$

where $h_0=(h_r+h_g+h_b)/3$ is the intensity of the reference image $\mathbf{h}$. If $v_1\approx v_2\approx v_3$, then the condition in Proposition 2.1 is satisfied, that is $v_i/h_0, i\in\{1,2,3\}$ approximate the constant a, so that $\mathbf{u}$ will respect the hue of $\mathbf{h}$. In the following section, $h_k/h_0, k\in\{r,g,b\}$ will be written as A_k, and the hue will be approximately preserved by penalizing

$$\tilde{H}(\mathbf{v})=\int_\Omega\left[(v_1-v_2)^2+(v_2-v_3)^2+(v_3-v_1)^2\right]\mathrm{d}x\mathrm{d}y.$$

2.2 Saturation-value total variation

Jia, Ng and Wang [11] proposed SV-TV regularization for color image restoration. The idea is to make use of neighborhood color pixel values in saturation and value components to control regularization in color image restoration. SV-TV is given as follows:

$$\begin{aligned}\text{SV-TV}(\mathbf{u}) = &\int_\Omega \sqrt{|\partial_x \mathbf{u}(x,y)|_s^2 + |\partial_y \mathbf{u}(x,y)|_s^2}\,\mathrm{d}x\mathrm{d}y \\ &+\mu\sqrt{|\partial_x \mathbf{u}(x,y)|_v^2 + |\partial_y \mathbf{u}(x,y)|_v^2}\,\mathrm{d}x\mathrm{d}y,\end{aligned}$$

where μ is a positive parameter given as the weight of the value component. Let

$$\partial_x \mathbf{u}(x,y)^\top = \begin{bmatrix}\partial_x u_r(x,y)\\ \partial_x u_g(x,y)\\ \partial_x u_b(x,y)\end{bmatrix}, \quad \partial_y \mathbf{u}(x,y)^\top = \begin{bmatrix}\partial_y u_r(x,y)\\ \partial_y u_g(x,y)\\ \partial_y u_b(x,y)\end{bmatrix}, \quad W = \begin{bmatrix}2 & -1 & -1\\ -1 & 2 & -1\\ -1 & -1 & 2\end{bmatrix},$$

then

$$\begin{aligned}&|\partial_x \mathbf{u}(x,y)|_s = \frac{1}{3}\left\|W\partial_x \mathbf{u}(x,y)^\top\right\|, \quad |\partial_y \mathbf{u}(x,y)|_s = \frac{1}{3}\left\|W\partial_y \mathbf{u}(x,y)^\top\right\|,\\ &|\partial_x \mathbf{u}(x,y)|_v = \frac{1}{\sqrt{3}}|\partial_x u_r(x,y) + \partial_x u_g(x,y) + \partial_x u_b(x,y)|,\\ &|\partial_y \mathbf{u}(x,y)|_v = \frac{1}{\sqrt{3}}|\partial_y u_r(x,y) + \partial_y u_g(x,y) + \partial_y u_b(x,y)|,\end{aligned}$$

where $\partial_x u_k$ (or $\partial_y u_k$) is the partial derivative of u_k with respect to x (or y).

3 The proposed hue-preserving model

In this section, we make use of the following notations to formulate the proposed hue-preserving SV-TV model:

$$\mathbf{f} = [f_r, f_g, f_b]^\top : \Omega \ \to \ [0,1]^3$$

represents the observed image, and f_r, f_g and f_b represents R, G and B channels of $\mathbf{f}$, respectively. $\mathbf{u}$ is the objective restored image and $\mathbf{h}$ represents the reference image for the hue preservation.

3.1 The formulation

The proposed hue-preserving SV-TV model is given as follows:

$$\begin{aligned}\min_{\mathbf{u},\mathbf{v},d}\ &\text{SV-TV}(\mathbf{u}) + \frac{\alpha_1}{2}\int_\Omega d^2\,\mathrm{d}x\mathrm{d}y + \frac{\alpha_2}{2}\int_\Omega \|K\star\mathbf{u}-\mathbf{f}\|^2\,\mathrm{d}x\mathrm{d}y\\ &+\frac{\alpha_3}{2}\int_\Omega [(v_1-v_2)^2+(v_2-v_3)^2+(v_3-v_1)^2]\,\mathrm{d}x\mathrm{d}y\\ \text{s.t.}\quad &u_r = A_r v_1 + d, \quad u_g = A_g v_2 + d, \quad u_b = A_b v_3 + d,\end{aligned} \tag{3.1}$$

where K is a given blurring operator, $\star$ is the convolution operation and $\alpha_1,\alpha_2,\alpha_3$ are positive parameters given as the weights of different terms of the proposed functional. The first term of (3.1) is the SV-TV regularization of $\mathbf{u}$ to eliminate the degradation. The aim of the second term ($\int_\Omega d^2\mathrm{d}x\mathrm{d}y$) of (3.1) is to make sure that the value of d is not too large. Otherwise, large d will perturb the RGB channels, which will lead to the increase of the brightness of the objective image. Therefore, d is penalized moderately by adjusting the parameter α_1 in the proposed model. The third term ($\int_\Omega \|K\star\mathbf{u}-\mathbf{f}\|^2\mathrm{d}x\mathrm{d}y$) is the fidelity term between the objective restored image and the observed input image. The fourth term is the proposed hue-preserving term. The aim of this term is to make sure that $v_1\approx v_2\approx v_3$. As is shown in Section 2.1, the restored image $\mathbf{u}$ will have a similar hue with the reference image $\mathbf{h}$ in this case.

In order to solve the proposed model efficiently, we consider the equivalent form of (3.1) in the following discussion. We first introduce three matrices $C,\mathbf{A}$ and H as

$$C=\begin{bmatrix}1&-1&0\\0&1&-1\\-1&0&1\end{bmatrix},\quad \mathbf{A}=\begin{bmatrix}A_r&0&0\\0&A_g&0\\0&0&A_b\end{bmatrix},\quad H=\begin{bmatrix}1\\1\\1\end{bmatrix}.$$

Then the equivalent version of the fourth term and the constraints in (3.1) are given as

$$\int_\Omega \|C\mathbf{v}\|^2\mathrm{d}x\mathrm{d}y,\quad \mathbf{u}=\mathbf{A}\mathbf{v}+Hd.$$

Therefore, we derive the equivalent version of (3.1) as follows:

$$\begin{aligned}&\min_{\mathbf{u},\mathbf{v},d}\ \text{SV-TV}(\mathbf{u})+\frac{\alpha_1}{2}\int_\Omega d^2\mathrm{d}x\mathrm{d}y+\frac{\alpha_2}{2}\int_\Omega\|K\star\mathbf{u}-\mathbf{f}\|^2\mathrm{d}x\mathrm{d}y+\frac{\alpha_3}{2}\int_\Omega\|C\mathbf{v}\|^2\mathrm{d}x\mathrm{d}y\\&\text{s.t.}\quad \mathbf{u}=\mathbf{A}\mathbf{v}+Hd.\end{aligned}\tag{3.2}$$

We set the admissible set

$$\Lambda=\left\{(\mathbf{u},\mathbf{v},d)\,|\,\mathbf{u}=\mathbf{A}\mathbf{v}+Hd,u_r,u_g,u_b\in BV(\Omega),l_u\le u_k(x,y)\le L_u,v_1,v_2,v_3,d\in L^2(\Omega)\right\},$$

where $BV(\Omega)$ is the function space with bounded variation. For the proposed variational model (3.2), we have the following existence result about the solution.

Theorem 3.1. *Assume that $f_k\in L^\infty(\Omega),h_k\in L^\infty(\Omega)\cap BV(\Omega),k\in\{r,g,b\}$ and $0<l_h\le h_k(x,y)\le L_h$, then the minimization problem* (3.2) *has at least one solution $(\tilde{\mathbf{u}},\tilde{\mathbf{v}},\tilde{d})$ in the admissible set Λ for fixed $\alpha_1,\alpha_2,\alpha_3$.*

Proof. First, we set $\mathbf{u}=\mathbf{h},\mathbf{v}=h_0,d=0$, then the energy in (3.2) will be finite, which implies that the infimum of the energy must be finite. Suppose $(\mathbf{u}^n,\mathbf{v}^n,d^n)$ is a minimizing sequence of (3.2) in the admissible set Λ, then there exists a constant $Q>0$ such that

$$\text{SV-TV}(\mathbf{u}^n)\le Q.$$

Combining this with the boundedness of $u_r^n(x,y), u_g^n(x,y), u_b^n(x,y)$, we deduce that there exists a subsequence (also denoted by $u_r^n(x,y), u_g^n(x,y), u_b^n(x,y)$) and $\tilde{u_r}, \tilde{u_g}, \tilde{u_b} \in BV(\Omega)$ such that (see [11, Proposition 3.2])

$$\begin{aligned}
u_r^n(x,y) &\xrightarrow{L^1(\Omega)} \tilde{u_r}(x,y), \quad u_r^n(x,y) \to \tilde{u_r}(x,y) \quad \text{a.e.} \quad (x,y)\in\Omega,\\
u_g^n(x,y) &\xrightarrow{L^1(\Omega)} \tilde{u_g}(x,y), \quad u_g^n(x,y) \to \tilde{u_g}(x,y) \quad \text{a.e.} \quad (x,y)\in\Omega,\\
u_b^n(x,y) &\xrightarrow{L^1(\Omega)} \tilde{u_b}(x,y), \quad u_b^n(x,y) \to \tilde{u_b}(x,y) \quad \text{a.e.} \quad (x,y)\in\Omega,
\end{aligned} \tag{3.3}$$

and $l_u \le \tilde{u_k}(x,y) \le L_k$. Meanwhile, recall that $A_k = h_k/h_0$, then

$$\frac{3l_h}{2L+l_h} \le A_k \le \frac{3L}{L+2l_h},$$

which can be written as $l_A \le A_k \le L_A$. Noting that d^n is uniformly bounded in $L^2(\Omega)$, and $\mathbf{u} = \mathbf{A}\mathbf{v} + Hd$. We can easily deduce that v_1^n, v_2^n, v_3^n are also uniformly bounded in $L^2(\Omega)$. Then up to a subsequence, there exists $\tilde{v_1}, \tilde{v_2}, \tilde{v_3}, \tilde{d} \in L^2(\Omega)$ such that

$$\begin{aligned}
v_1^n(x,y) &\xrightarrow{L^1(\Omega)} \tilde{v_1}(x,y), \quad v_1^n(x,y) \to \tilde{v_1}(x,y) \quad \text{a.e.} \quad (x,y)\in\Omega,\\
v_2^n(x,y) &\xrightarrow{L^1(\Omega)} \tilde{v_2}(x,y), \quad v_2^n(x,y) \to \tilde{v_2}(x,y) \quad \text{a.e.} \quad (x,y)\in\Omega,\\
v_3^n(x,y) &\xrightarrow{L^1(\Omega)} \tilde{v_3}(x,y), \quad v_3^n(x,y) \to \tilde{v_3}(x,y) \quad \text{a.e.} \quad (x,y)\in\Omega,\\
d^n(x,y) &\xrightarrow{L^1(\Omega)} \tilde{d}(x,y), \quad d^n(x,y) \to \tilde{d}(x,y) \quad \text{a.e.} \quad (x,y)\in\Omega.
\end{aligned} \tag{3.4}$$

Combining (3.3) and (3.4) with the linear condition $\mathbf{u}^n = \mathbf{A}\mathbf{v}^n + d^n$, we obtain that $\tilde{\mathbf{u}} = \mathbf{A}\tilde{\mathbf{v}} + \tilde{d}$, which means $(\tilde{\mathbf{u}}, \tilde{\mathbf{v}}, \tilde{d}) \in \Lambda$.

As a consequence of the lower semicontinuity of SV-TV$(\mathbf{u})$, we have

$$\liminf \text{SV-TV}(\mathbf{u}^n) \ge \text{SV-TV}(\tilde{\mathbf{u}}). \tag{3.5}$$

Meanwhile, the following convergence results hold:

$$\begin{aligned}
\big((K\star u_r^n)(x,y) - f_r^n(x,y)\big)^2 &\to \big(K\star\tilde{u_r}(x,y) - f_r(x,y)\big)^2 \quad \text{a.e.} \quad (x,y)\in\Omega,\\
\big((K\star u_g^n)(x,y) - f_g^n(x,y)\big)^2 &\to \big(K\star\tilde{u_g}(x,y) - f_g(x,y)\big)^2 \quad \text{a.e.} \quad (x,y)\in\Omega,\\
\big((K\star u_b^n)(x,y) - f_b^n(x,y)\big)^2 &\to \big(K\star\tilde{u_b}(x,y) - f_b(x,y)\big)^2 \quad \text{a.e.} \quad (x,y)\in\Omega,\\
\big(v_1^n(x,y) - v_2^n(x,y)\big)^2 &\to \big(\tilde{v_1}(x,y) - \tilde{v_2}(x,y)\big)^2 \quad \text{a.e.} \quad (x,y)\in\Omega,\\
\big(v_2^n(x,y) - v_3^n(x,y)\big)^2 &\to \big(\tilde{v_2}(x,y) - \tilde{v_3}(x,y)\big)^2 \quad \text{a.e.} \quad (x,y)\in\Omega,\\
\big(v_3^n(x,y) - v_1^n(x,y)\big)^2 &\to \big(\tilde{v_3}(x,y) - \tilde{v_1}(x,y)\big)^2 \quad \text{a.e.} \quad (x,y)\in\Omega.
\end{aligned}$$

By using Fatou's lemma, we obtain

$$\begin{aligned}&\liminf\left\{\frac{\alpha_1}{2}\int_\Omega (d^n)^2\mathrm{d}x\mathrm{d}y+\frac{\alpha_2}{2}\int_\Omega \|K\star\mathbf{u}^n-\mathbf{f}\|^2\mathrm{d}x\mathrm{d}y+\frac{\alpha_3}{2}\int_\Omega \|C\mathbf{v}^n\|^2\mathrm{d}x\mathrm{d}y\right\}\\ \geq&\frac{\alpha_1}{2}\int_\Omega \tilde{d}^2\mathrm{d}x\mathrm{d}y+\frac{\alpha_2}{2}\int_\Omega \|K\star\tilde{\mathbf{u}}-\mathbf{f}\|^2\mathrm{d}x\mathrm{d}y+\frac{\alpha_3}{2}\int_\Omega \|C\tilde{\mathbf{v}}\|^2\mathrm{d}x\mathrm{d}y. \end{aligned}\tag{3.6}$$

Combining (3.5) with (3.6) , we derive

$$\begin{aligned}&\liminf\left\{\text{SV-TV}(\mathbf{u}^n)+\frac{\alpha_1}{2}\int_\Omega (d^n)^2\mathrm{d}x\mathrm{d}y\right.\\ &\qquad\left.+\frac{\alpha_2}{2}\int_\Omega \|K\star\mathbf{u}^n-\mathbf{f}\|^2\mathrm{d}x\mathrm{d}y+\frac{\alpha_3}{2}\int_\Omega \|C\mathbf{v}^n\|^2\mathrm{d}x\mathrm{d}y\right\}\\ \geq&\text{SV-TV}(\tilde{\mathbf{u}})+\frac{\alpha_1}{2}\int_\Omega \tilde{d}^2\mathrm{d}x\mathrm{d}y+\frac{\alpha_2}{2}\int_\Omega \|K\star\tilde{\mathbf{u}}-\mathbf{f}\|^2\mathrm{d}x\mathrm{d}y+\frac{\alpha_3}{2}\int_\Omega \|C\tilde{\mathbf{v}}\|^2\mathrm{d}x\mathrm{d}y,\end{aligned}$$

which leads to the existence of the solution of (3.2). □

3.2 The illustration

In this subsection, we will show the hue-preserving effect of the proposed model (3.2). We generate the degraded image by adding a Gaussian noise with a standard deviation of 1 to the hue channel of the original color image. As is shown in Fig. 1, the overall color of the original image has been completely changed because the distortion is added to the hue channel directly. In the proposed model, we make use of a blurred version of the original color image as the reference image for hue preservation. In Fig. 1, we display the original color image, the degraded color image, the restored result by using SV-TV model [11], the restored result by using the proposed model respectively. We see from

Figure 1: From left to right: the original color image, the degraded color image, the restored result by using SV-TV model, the restored result by using the proposed model.

the figure that the restored result by using SV-TV model remains the overall color of the degraded image. However, the restored result by using the proposed model keeps the overall color corresponding to the hue information of the original image, which illustrates the hue-preserving effect of the proposed color image restoration model.

4 Numerical algorithm

In this section, we consider the discrete version of (3.2) and present an efficient algorithm to solve the proposed optimization problem. We first reshape each channel of a color image to a vector of length $n = M \times N$. We write the discrete version of d as $\mathbf{d} \in \mathbb{R}^n$ and keep the notations, $\mathbf{u} \in \mathbb{R}^{3n}, \mathbf{v} \in \mathbb{R}^{3n}$ and $\mathbf{A} = \text{diag}\{A_r, A_g, A_b\} \in \mathbb{R}^{3n \times 3n}$, unchanged in the following discussion. Then the discrete differential operators $\mathbf{D}_x$ and $\mathbf{D}_y$ can be defined as

$$\mathbf{D}_x := I_3 \otimes I_N \otimes D_M, \quad \mathbf{D}_y := I_3 \otimes D_N \otimes I_M,$$

where $\otimes$ denotes the Kronecker product, I_N is an identity matrix of size $N \times N$ and

$$D_M := \begin{bmatrix} -1 & 1 & & \\ & \ddots & \ddots & \\ & & -1 & 1 \\ 1 & & & -1 \end{bmatrix} \in \mathbb{R}^{M \times M},$$

K, W, C and $\mathbf{H}$ can be similarly defined as

$$\mathbf{K} = K \otimes I_n, \quad \mathbf{W} = W \otimes I_n, \quad \mathbf{C} = C \otimes I_n, \quad \mathbf{H} = [1,1,1]^\top \otimes I_n.$$

We remark here that we consider the periodic boundary condition in practice. As a result, the discrete version of SV-TV$(\mathbf{u})$ is given as

$$\text{SV-TV}(\mathbf{u}) = \|\mathbf{D}_s \mathbf{u}\|_{2,1} + \alpha \|\mathbf{D}_v \mathbf{u}\|_{2,1},$$

where $\|A\|_{2,1}$ represents the $l_{2,1}$ norm of matrix $A = (a_{i,j})$ and is defined as the sum of l_2 norms of each row, namely,

$$\|A\|_{2,1} = \sum_i \sqrt{\sum_j a_{i,j}^2},$$

and

$$\mathbf{D}_s \mathbf{u} = \frac{1}{3} \begin{bmatrix} \mathbf{H}^\top \mathbf{W} \mathbf{D}_x \mathbf{u} & \mathbf{H}^\top \mathbf{W} \mathbf{D}_y \mathbf{u} \end{bmatrix}, \quad \mathbf{D}_v \mathbf{u} = \frac{1}{\sqrt{3}} \begin{bmatrix} \mathbf{H}^\top \mathbf{D}_x \mathbf{u} & \mathbf{H}^\top \mathbf{D}_y \mathbf{u} \end{bmatrix}.$$

The discrete version of (3.2) is

$$\begin{aligned} &\min_{\mathbf{u},\mathbf{v},\mathbf{d}} \text{SV-TV}(\mathbf{u}) + \frac{\alpha_1}{2} \|\mathbf{d}\|^2 + \frac{\alpha_2}{2} \|\mathbf{K}\mathbf{u} - \mathbf{f}\|^2 + \frac{\alpha_3}{2} \|\mathbf{C}\mathbf{v}\|^2 \\ &\text{s.t.} \quad \mathbf{u} = \mathbf{A}\mathbf{v} + \mathbf{H}\mathbf{d}. \end{aligned} \tag{4.1}$$

By introducing the Lagrangian multiplier, the augmented Lagrangian of the above optimization problem is given as

$$\begin{aligned}\mathcal{L}=&\text{SV-TV}(\mathbf{u})+\frac{\alpha_1}{2}\|\mathbf{d}\|^2+\frac{\alpha_2}{2}\|\mathbf{Ku}-\mathbf{f}\|^2+\frac{\alpha_3}{2}\|\mathbf{Cv}\|^2\\&+\langle\lambda,\mathbf{u}-\mathbf{Av}-\mathbf{Hd}\rangle+\frac{\beta}{2}\|\mathbf{u}-\mathbf{Av}-\mathbf{Hd}\|^2,\end{aligned}$$

where $\beta>0$ is a penalty parameter and $\lambda\in\mathbb{R}^{3n}$ is a Lagrange multiplier. Then the proposed minimization problem can be solved by an ADMM-based algorithms for three-block separable convex programming [9]. We conclude it in the Algorithm 1.

For the convergence of Algorithm A, we have the following theorem which can be proved by using the similar arguments in [9].

Theorem 4.1. *Let* $\{z^l\}_{l\in\mathbb{N}}=\{(\mathbf{u}^l,\mathbf{v}^l,\mathbf{d}^l)\}_{l\in\mathbb{N}}$ *be a sequence generated by Algorithm* 1. *Then the sequence* $\{z^l\}_{l\in\mathbb{N}}$ *converges to a critical point* $z^*=(\mathbf{u}^*,\mathbf{v}^*,\mathbf{d}^*)$ *of problem* (4.1).

Algorithm 1. Algorithm A.

Step 1. Set the stopping criteria ϵ and initialization $\mathbf{u}^0,\mathbf{v}^0,\mathbf{d}^0$.

Step 2. For fixed $\mathbf{v}^n,\mathbf{d}^n$, update $\tilde{\mathbf{u}}^n$ by solving

$$\begin{aligned}\min_{\mathbf{u}}\Big\{&\text{SV-TV}(\mathbf{u})+\frac{\alpha_2}{2}\|\mathbf{Ku}-\mathbf{f}\|^2\\&+\langle\lambda^n,\mathbf{u}-\mathbf{Av}^n-\mathbf{Hd}^n\rangle+\frac{\beta}{2}\|\mathbf{u}-\mathbf{Av}^n-\mathbf{Hd}^n\|^2\Big\}.\end{aligned}\tag{4.2}$$

Step 3. For fixed $\tilde{\mathbf{u}}^n,\mathbf{d}^n$, update $\tilde{\mathbf{v}}^n$ by solving

$$\min_{\mathbf{v}}\Big\{\frac{\alpha_3}{2}\|\mathbf{Cv}\|^2+\langle\lambda^n,\tilde{\mathbf{u}}^n-\mathbf{Av}-\mathbf{Hd}^n\rangle+\frac{\beta}{2}\|\tilde{\mathbf{u}}^n-\mathbf{Av}-\mathbf{Hd}^n\|^2\Big\}.\tag{4.3}$$

Step 4. For fixed $\tilde{\mathbf{u}}^n,\tilde{\mathbf{v}}^n$, update $\tilde{\mathbf{d}}^n$ by solving

$$\min_{\mathbf{d}}\Big\{\frac{\alpha_1}{2}\|\mathbf{d}\|^2+\langle\lambda^n,\tilde{\mathbf{u}}^n-\mathbf{A}\tilde{\mathbf{v}}^n-\mathbf{Hd}\rangle+\frac{\beta}{2}\|\tilde{\mathbf{u}}^n-\mathbf{A}\tilde{\mathbf{v}}^n-\mathbf{Hd}\|^2\Big\}.\tag{4.4}$$

Step 5. Update $\tilde{\lambda}^n$ by using $\tilde{\lambda}^n=\lambda^n+\beta(\tilde{\mathbf{u}}^n-\mathbf{A}\tilde{\mathbf{v}}^n-\mathbf{H}\tilde{\mathbf{d}}^n)$.

Step 6. Generate new $\mathbf{u}^{n+1},\mathbf{v}^{n+1},\mathbf{d}^{n+1},\lambda^{n+1}$ by using $\mathbf{v}^{n+1}=\tilde{\mathbf{v}}^n$,

$$\begin{bmatrix}\mathbf{u}^{n+1}\\\mathbf{d}^{n+1}\\\lambda^{n+1}\end{bmatrix}=\begin{bmatrix}\mathbf{u}^{n}\\\mathbf{d}^{n}\\\lambda^{n}\end{bmatrix}-\frac{3}{4}\begin{bmatrix}I_{3n}&\mathbf{H}/2&0\\-\mathbf{H}^\top/2&I_n&0\\0&0&I_{3n}\end{bmatrix}\begin{bmatrix}\mathbf{u}^{n}-\tilde{\mathbf{u}}^{n}\\\mathbf{d}^{n}-\tilde{\mathbf{d}}^{n}\\\lambda^{n}-\tilde{\lambda}^{n}\end{bmatrix}.$$

Step 7. Iterate the above steps until $(\|\mathbf{u}^{n+1}-\mathbf{u}^n\|^2)/\|\mathbf{u}^n\|^2\le\epsilon$.

4.1 The subproblem (4.2)

In this subsection, we present the details about how to solve subproblem (4.2). We first rewrite subproblem (4.2) as follows:

$$\min_{\mathbf{u}}\left\{\text{SV-TV}(\mathbf{u})+\frac{\alpha_2}{2}\|\mathbf{K}\mathbf{u}-\mathbf{f}\|^2+\frac{\beta}{2}\left\|\mathbf{u}-\mathbf{A}\mathbf{v}^n-\mathbf{H}\mathbf{d}^n+\frac{\lambda^n}{\beta}\right\|^2\right\}. \tag{4.5}$$

As is discussed in [11], we introduce the following linear transformation:

$$\mathbf{P}=\begin{bmatrix}\frac{1}{\sqrt{2}} & -\frac{1}{\sqrt{2}} & 0\\ \frac{1}{\sqrt{6}} & \frac{1}{\sqrt{6}} & -\frac{2}{\sqrt{6}}\\ \frac{1}{\sqrt{3}} & \frac{1}{\sqrt{3}} & \frac{1}{\sqrt{3}},\end{bmatrix}\otimes I_n,\quad \mathbf{q}=\begin{bmatrix}q_r\\ q_g\\ q_b\end{bmatrix}=\mathbf{P}\begin{bmatrix}u_r\\ u_g\\ u_b\end{bmatrix},$$

then the discrete version of subproblem (4.5) is equivalent to

$$\begin{aligned}\min_{\mathbf{q}}\sum_{i=1}^{m}\sum_{j=1}^{n}\Bigg(&\sqrt{(\mathbf{D}_x\boldsymbol{q}_1)_{ij}^2+(\mathbf{D}_x\boldsymbol{q}_2)_{ij}^2+(\mathbf{D}_y\boldsymbol{q}_1)_{ij}^2+(\mathbf{D}_y\boldsymbol{q}_2)_{ij}^2}\\ &+\mu\sqrt{(\mathbf{D}_x\boldsymbol{q}_3)_{ij}^2+(\mathbf{D}_y\boldsymbol{q}_3)_{ij}^2}\Bigg)+\frac{\alpha_2}{2}\|\tilde{\mathbf{K}}\mathbf{q}-\tilde{\mathbf{f}}\|_2^2+\frac{\beta}{2}\|\mathbf{q}-\tilde{\mathbf{z}}\|_2^2,\end{aligned} \tag{4.6}$$

where

$$\tilde{\mathbf{K}}=\mathbf{P}\mathbf{K}\mathbf{P}^\top,\quad \tilde{\mathbf{f}}=\mathbf{P}\mathbf{f},\quad \tilde{\mathbf{z}}=\mathbf{P}\left(\mathbf{A}\mathbf{v}^n+\mathbf{H}\mathbf{d}^n-\frac{\lambda^n}{\beta}\right).$$

We remark that the above optimization problem can be solved efficiently by using primal-dual method, see [11] for details.

4.2 The subproblems (4.3) and (4.4)

In this subsection, we present the details about how to solve subproblems (4.3) and (4.4). As is discussed in the previous section, we rewrite the subproblems (4.3) and (4.4) as

$$\begin{aligned}&\min_{\mathbf{v}}\left\{\frac{\alpha_3}{2}\|\mathbf{C}\mathbf{v}\|^2+\frac{\beta}{2}\left\|\tilde{\mathbf{u}}^n-\mathbf{A}\mathbf{v}-\mathbf{H}\mathbf{d}^n+\frac{\lambda^n}{\beta}\right\|^2\right\},\\ &\min_{\mathbf{d}}\left\{\frac{\alpha_1}{2}\|\mathbf{d}\|^2+\frac{\beta}{2}\left\|\tilde{\mathbf{u}}^n-\mathbf{A}\tilde{\mathbf{v}}^n-\mathbf{H}\mathbf{d}+\frac{\lambda^n}{\beta}\right\|^2\right\}.\end{aligned}$$

Then the closed-form solutions of $\tilde{\mathbf{v}}^n$ and $\tilde{\mathbf{d}}^n$ are given as

$$\begin{aligned}\tilde{\mathbf{v}}^n&=\left(\alpha_3\mathbf{C}^\top\mathbf{C}+\beta\mathbf{A}^\top\mathbf{A}\right)^{-1}\mathbf{A}^\top(\beta\tilde{\mathbf{u}}^n-\beta\mathbf{H}\mathbf{d}^n+\lambda^n),\\ \tilde{\mathbf{d}}^n&=\left(\alpha_1 I_n+\beta\mathbf{H}^\top\mathbf{H}\right)^{-1}\mathbf{H}^\top(\beta\tilde{\mathbf{u}}^n-\beta\mathbf{A}\tilde{\mathbf{v}}^n+\lambda^n).\end{aligned}$$

5 Numerical experiments

In this section, we present the numerical results to demonstrate the effectiveness of the proposed model and algorithm. We compare VTV [19], GVTV [17], CTV [4], SV-TV [11] and the proposed method for image restoration on several testing images. For each method, we solve the corresponding optimization problem with a range of different parameters and only report the best result in terms of PSNR values in the following evaluation. For the proposed model, we will test the effect of different parameters in Section 5.1. For the stopping criteria, we break the iteration when the relative error is less than or equal to 10^{-6} for all the testing methods. The proposed algorithm is implemented in MATLAB. All the computations are performed on a PC with an Intel(R) Core(TM) i7-7700HQ 2.80 GHz CPU. The quality of the recovered images is measured by

- SSIM index [21] which has been proven to be consistent with human eye perception,
- PSNR index which is the most common and widely used objective measurement to evaluate image quality,
- the S-CIELAB color metric [23] which includes a spatial processing step and is useful and efficient for measuring color reproduction errors of digital images.

5.1 The reference image and the parameters

In the proposed model, we need a reference image for hue preservation. However, the hue information of the degraded color image has been corrupted, see the example shown in Fig. 2(a). Therefore, we first make use of S-TV regularization introduced in [11] to

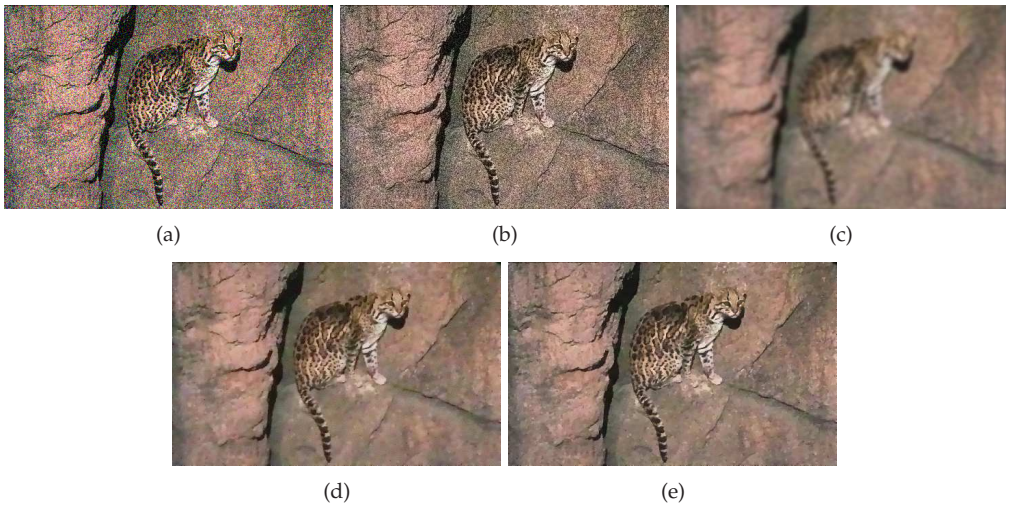

(a) (b) (c)

(d) (e)

Figure 2: An example of the reference image. (a) the degraded image, (b) the image processed by using S-TV regularization, (c) the image filtered by using a Gaussian filter, (d) the restored result with (b) as the reference image, (e) the restored result with (c) as the reference image.

eliminate the hue distortion of the degraded color image. The corresponding result is given in Fig. 2(b). We see from the result that the color distortion has been significantly reduced, and most of the noise exists only in the value channel. In order to make the hue preservation to be consistent, we then process the result by using a Gaussian filter and make use of the filtered result in Fig. 2(c) as the reference image in practice. In Figs. 2(d) and 2(e), we display the restored results by using the reference image with or without Gaussian filtering. We see that the hue preservation effect will be seriously disturbed by noise. Finally, we remark here that the proposed model is robust to the degree of the regularization and the filtering, which has been verified by extensive experiments.

We then study the effect of the parameters (α_1,α_2 and α_3) of the proposed model based on a color image degraded by a Gaussian noise with standard deviation 0.2. First, we set $\alpha_2=\alpha_3=1$ and $\alpha_1=0.00001,0.01,1,100$ and 100000, respectively. Recall that α_1 controls the penalty of the variable d. According to the experimental results displayed in the first row of Fig. 3, we find that α_1 influences the brightness of the restored image. As the value

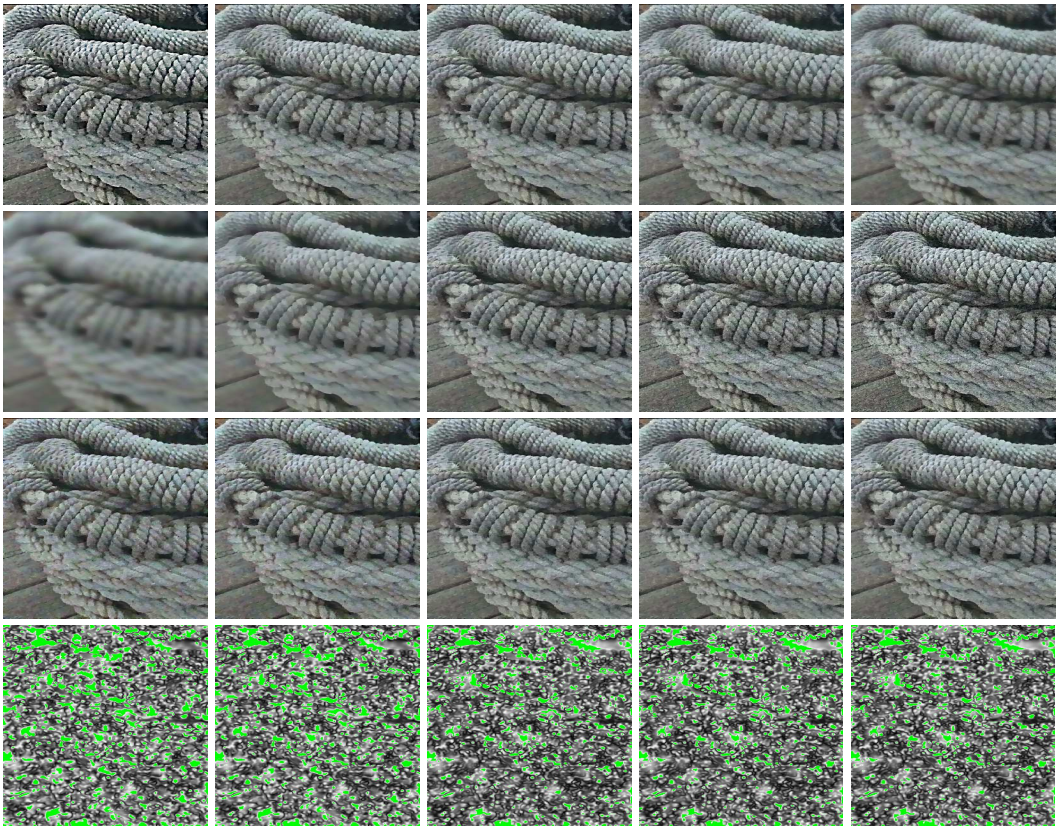

Figure 3: The first row: the restored results with different setting of α_1 $(0.00001,0.01,1,100,100000)$. The second row: the restored results with different setting of α_2 $(0.1,0.5,1,1.5,2)$. The third row: the restored results with different setting of α_3 $(0.00001,0.001,0.1,10,1000)$. The forth row: the spatial distributions of pixels with S-CIELAB color error corresponding to the results in the third row.

of α_1 gets smaller, the regularization of d is weaker which results in the larger disturbance in d and the increase of the brightness. When the value of α_1 is large, the restored image tends to be close to the channel average of the reference image, which results in blurring. See the restored results in the first row of Fig. 3 for more details. Then we set $\alpha_1 = \alpha_3 = 1$ and $\alpha_2 = 0.1,0.5,1,1.5$ and 2 respectively. Recall that α_2 controls the contribution of the fidelity term, which means that the larger the value of α_2, the closer the restored result is to the input degraded image. See the restored results in the second row of Fig. 3 for more details. Finally, we set $\alpha_1 = \alpha_2 = 1$ and $\alpha_3 = 0.00001,0.001,0.1,10$ and 1000 respectively. Recall that α_3 controls the hue-preserving term, we find that larger α_3 corresponds to better hue-preserving effect. See the restored results in the third row of Fig. 3 for more details. We also show the spatial distributions of pixels with S-CIELAB color error (larger than 5 units) in the forth row of Fig. 3, we see from the results that as α_3 increases, the pixel numbers (green region) with color error decreases. We report that the pixel numbers are 18455,17061,12278,12107 and 12108 corresponding to $\alpha_3 = 0.00001,0.001,0.1,10$ and 1000, respectively, which is consistent with our observation of the spatial distribution pictures.

5.2 Image denoising

In this test, we make use of 10 images in Fig. 4 taken from the Berkeley Segmentation Database5 [12] to test the proposed model for image denoising with respect to different noise levels. We artificially add Gaussian noises of standard deviation 0.2 and 0.3 to the ten groundtruth images in each channel and compute the SSIM, PSNR and S-CIELAB color metric values for each restored result by comparing it to the noise-free data. We compare the proposed model with some classical/novel methods including VTV [19], GVTV [17], CTV [2] and SV-TV [11], and we choose the optimal value of the parameters in terms of PSNR values for each testing method.

As examples of our experiment, we display some restored results in Figs. 5-8. We observe that the restored results by using the proposed method are significantly better than those by using other methods in terms of visual quality especially in reducing color distortions. Because there is no/less coupling of color channels, the restored results by using VTV, GVTV, CTV are clearly worse in reducing color artifacts. The visual quality of the restored results by using SV-TV has significant improvement. However, due to the introduction of the hue-preserving technique, the restored results by using the proposed model is the best visually compared with other testing methods, see the corresponding zooming parts especially the rope surface in Fig. 5, the rock surface in Fig. 6 and the water ripples in Fig. 7. We also display the spatial distributions of the pixels with color error (larger than 5 units, marked by green color) between the restored zooming parts and the ground-truth zooming parts in Figs. 5-8. We see clearly that the restored results by using the proposed model is the best in terms of color preserving.

We then report the PSNR values, the SSIM values, and the S-CIELAB color metric values of Figs. 5-8 and the average values of all 20 degraded images in Table 1. We see from the results that the proposed model always provide the best values. Meanwhile, we

Figure 4: Ground-truth images.

show the spatial distributions of PSNR, SSIM, and S-CIELAB color metric values of all 20 degraded images in Fig. 9. We see from the result that the proposed model is the best in terms of PSNR, SSIM, and S-CIELAB color error values.

5.3 Image deblurring

In this subsection, we test the performance of the proposed model for non-blind image deblurring. The degraded images are generated by convoluting the ground-truth images with a Gaussian kernel of standard deviation 1 and further adding Gaussian noises of standard deviation 0.2/0.3. As examples of the experiments, we show some restored results in Figs. 10-12. Again we display the spatial distributions of the pixels with color error (larger than 5 units, marked by green color) between the restored zooming parts and the ground-truth zooming parts in Figs. 10-12. We also see clearly from the figures that the restored results by using the proposed model is the best in terms of color/hue preserving. As expected, the proposed model has very good performance in reducing

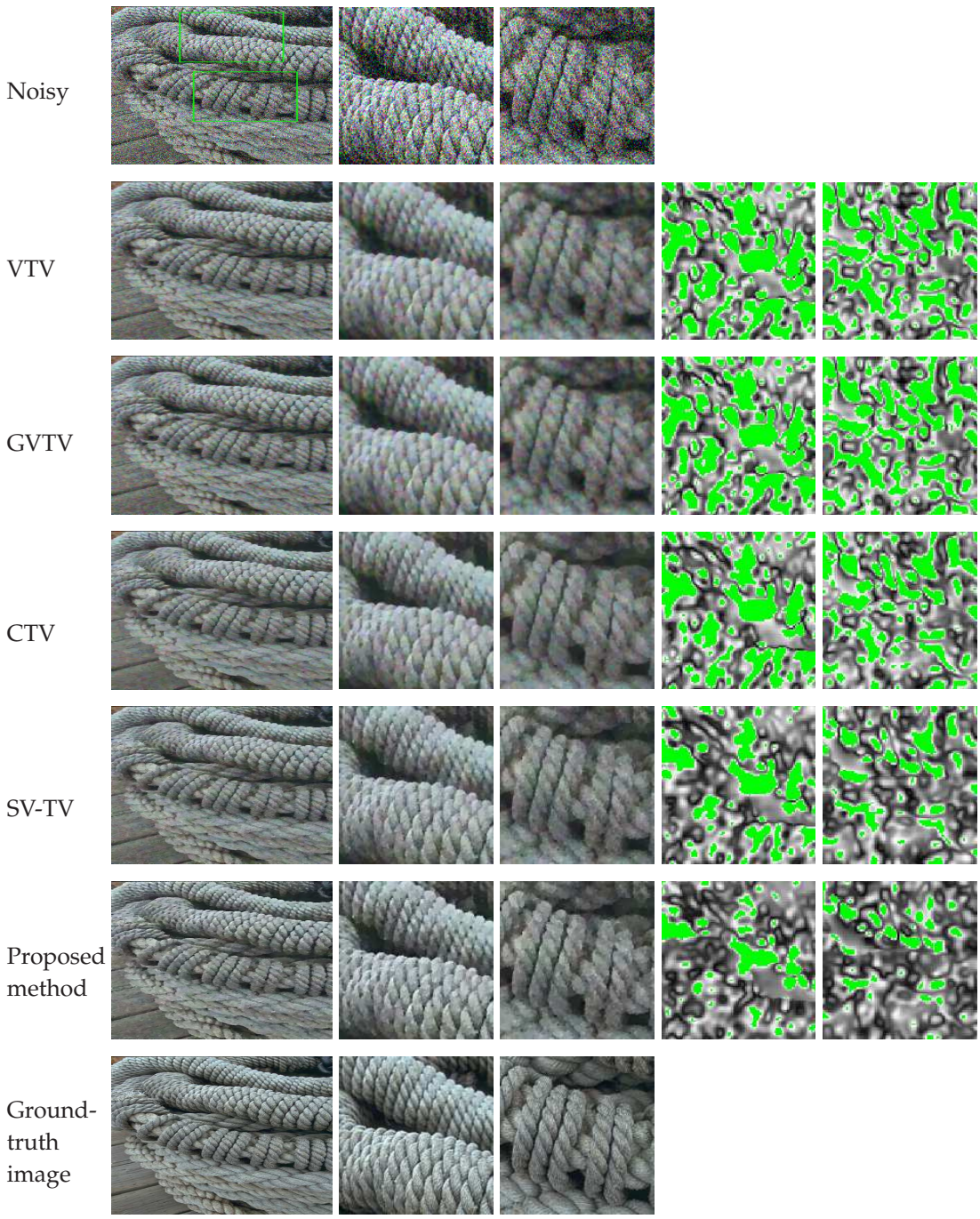

Figure 5: From top to bottom: the noisy image with $\sigma = 0.2$, restored results by using VTV, GVTV, CTV, SV-TV, the proposed method, and the ground-truth image. The corresponding zooming parts are displayed in the second column and the third column. The fourth column and fifth column are the spatial distributions of pixels with S-CIELAB error of the zooming parts.

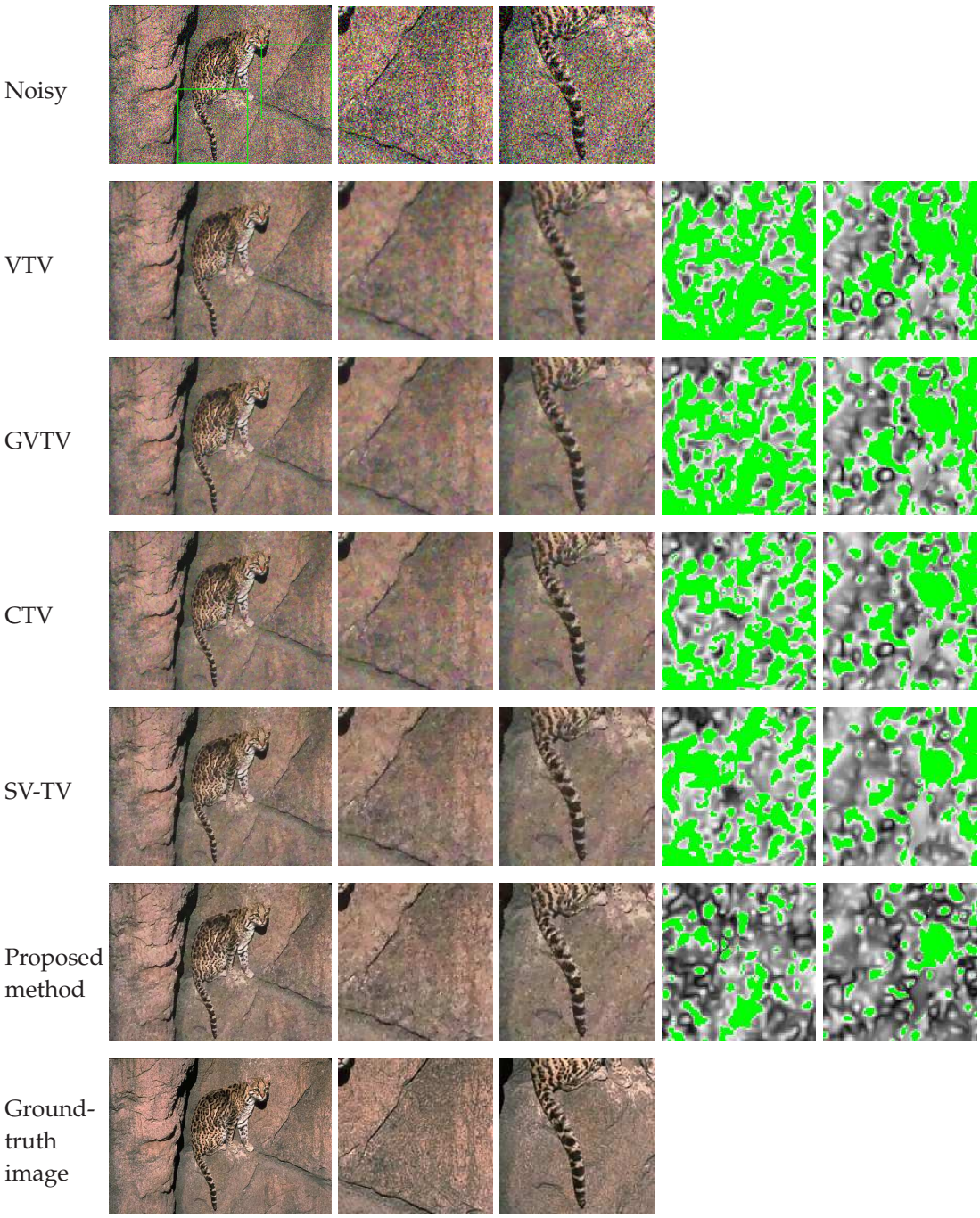

Figure 6: From top to bottom: the noisy image with $\sigma = 0.2$, restored results by using VTV, GVTV, CTV, SV-TV, the proposed method, and the ground-truth image. The corresponding zooming parts are displayed in the second column and the third column. The fourth column and fifth column are the spatial distributions of pixels with S-CIELAB error of the zooming parts.

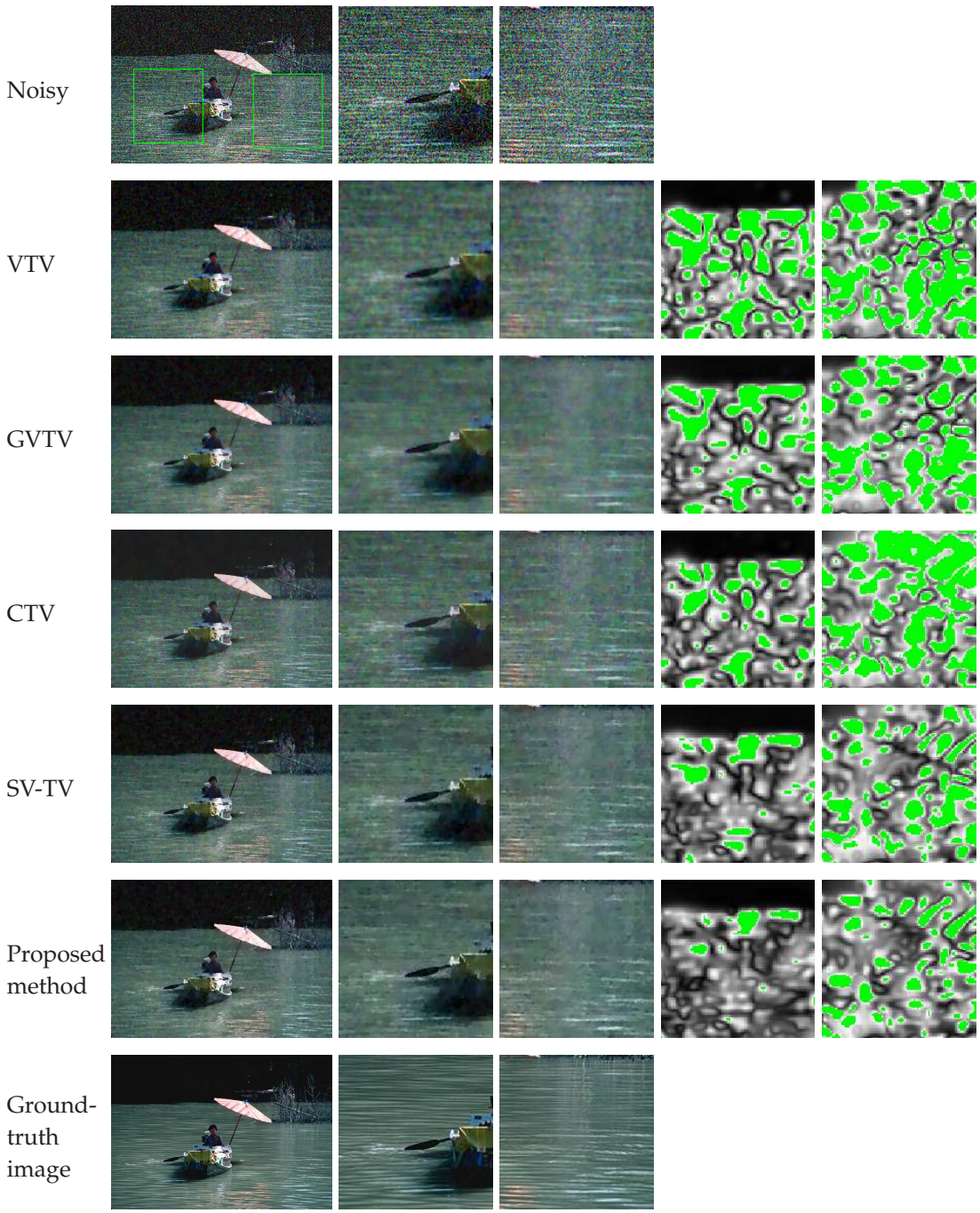

Figure 7: From top to bottom: the noisy image with $\sigma = 0.2$, restored results by using VTV, GVTV, CTV, SV-TV, the proposed method, and the ground-truth image. The corresponding zooming parts are displayed in the second column and the third column. The fourth column and fifth column are the spatial distributions of pixels with S-CIELAB error of the zooming parts.

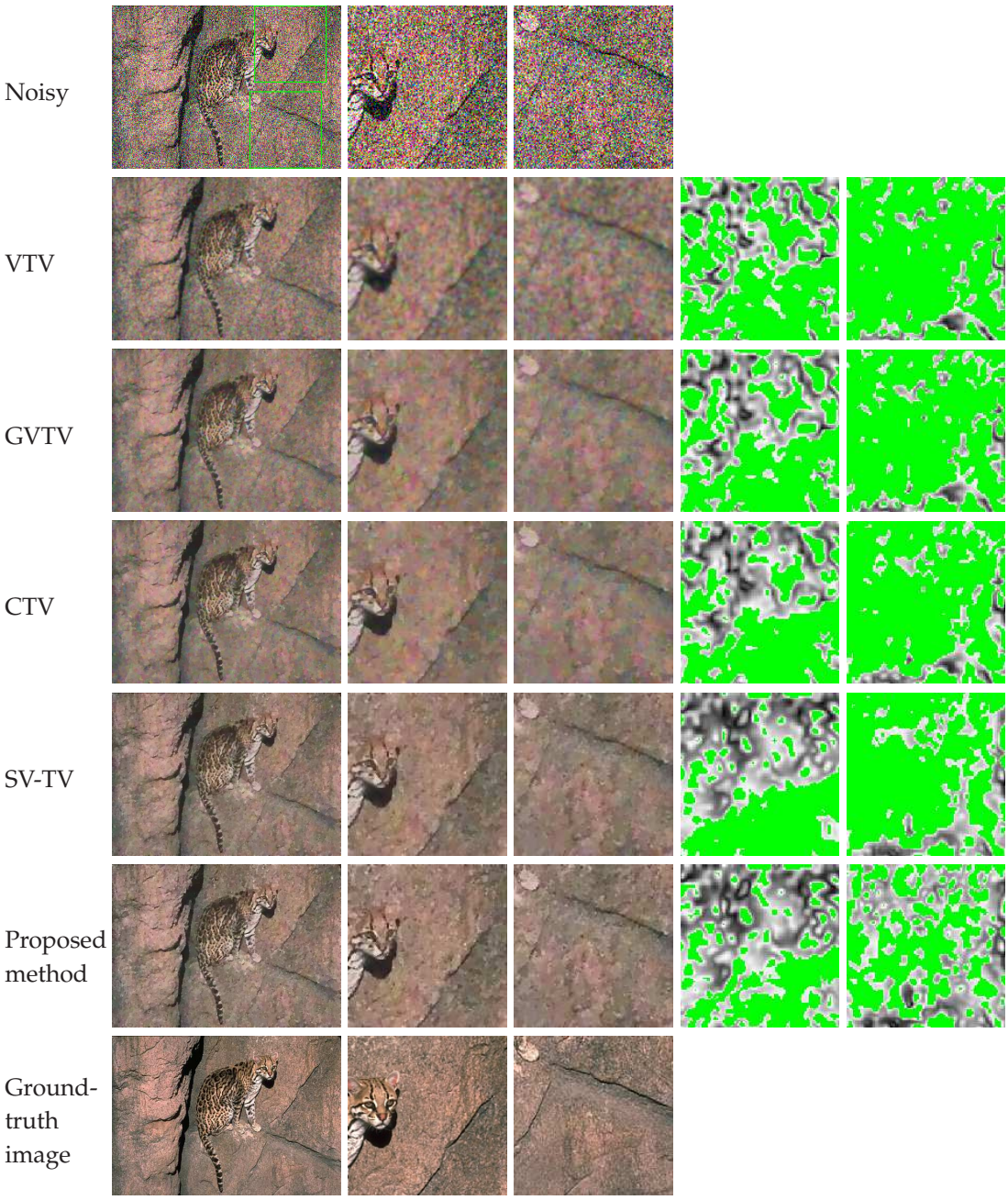

Figure 8: From top to bottom: the noisy image with $\sigma = 0.3$, restored results by using VTV, GVTV, CTV, SV-TV, the proposed method, and the ground-truth image. The corresponding zooming parts are displayed in the second column and the third column. The fourth column and fifth column are the spatial distributions of pixels with S-CIELAB error of the zooming parts.

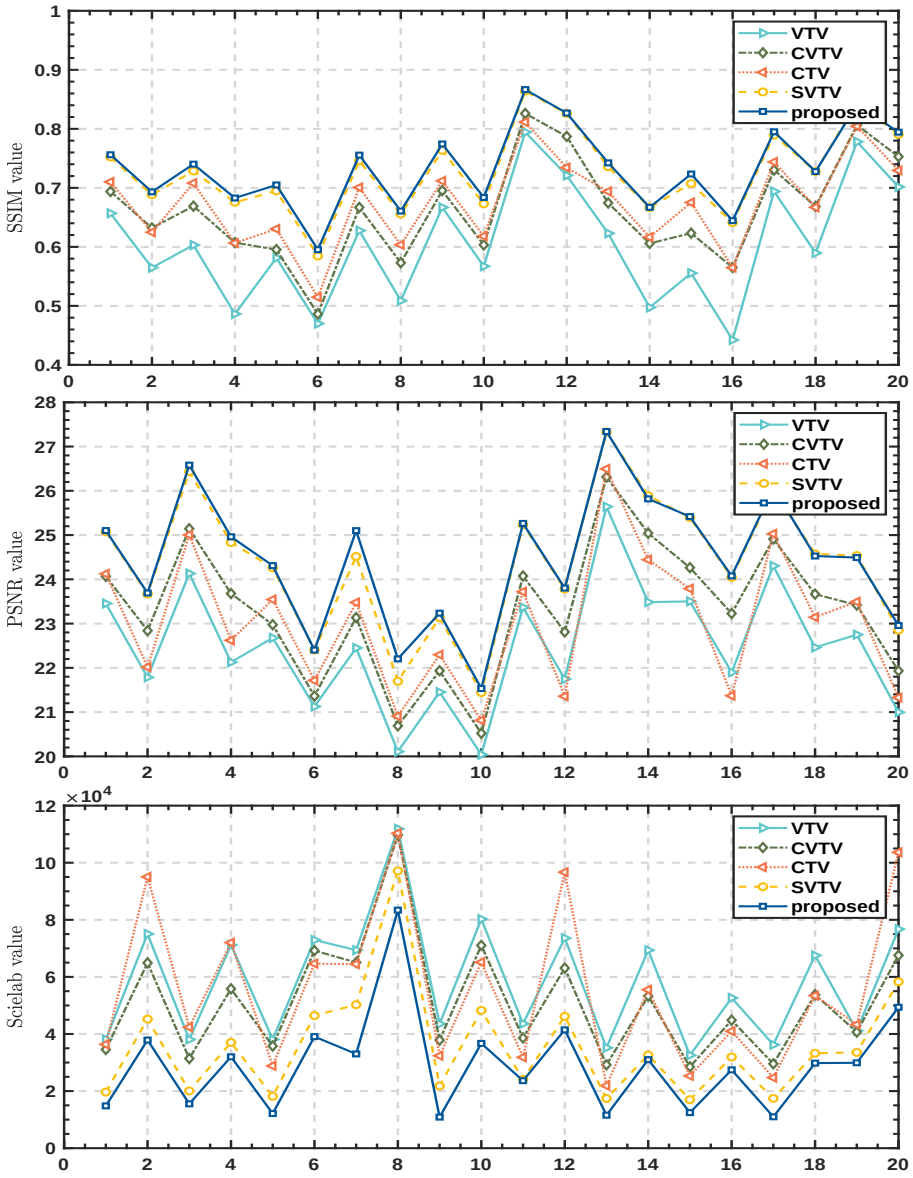

Figure 9: The spatial distributions of SSIM, PSNR and S-CIELAB color error values (between the ground-truth images and the restored results).

color artifacts, see especially the zooming parts. We also report PSNR, SSIM, and S-CIELAB color metric values in Table 2 and show the spatial distributions of PSNR, SSIM, and S-CIELAB color error values in Fig. 13. Again we see from the results that the proposed method is very competitive in terms of the visual quality and PSNR, SSIM, and S-CIELAB color error values.

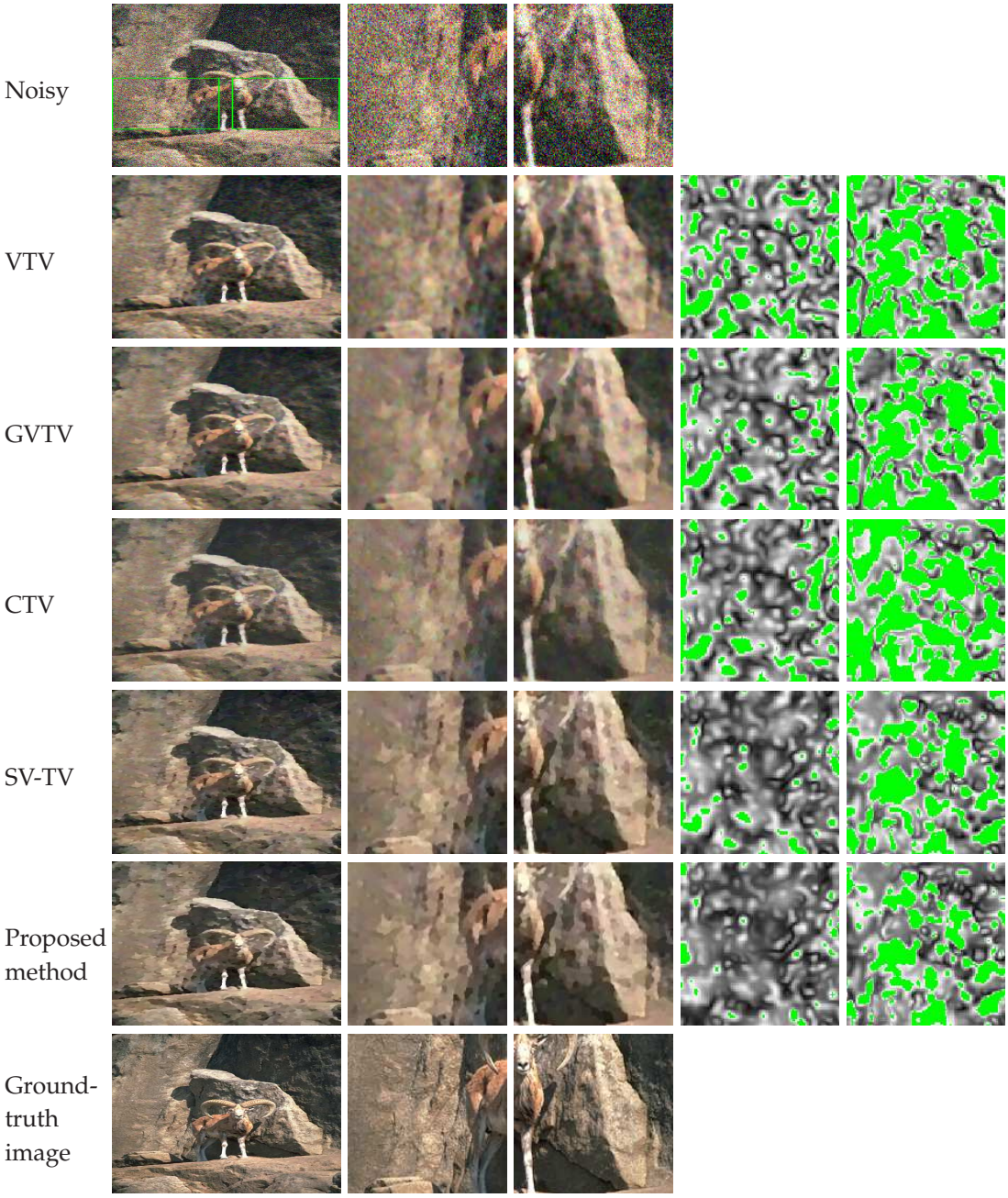

Figure 10: From top to bottom: the blurred and noisy image, the restored results by using VTV, GVTV, CTV, SV-TV, the proposed method, and the ground-truth image. The corresponding zooming parts are displayed in the second column and the third column. The fourth column and fifth column are the spatial distributions of pixels with S-CIELAB error of the zooming parts.

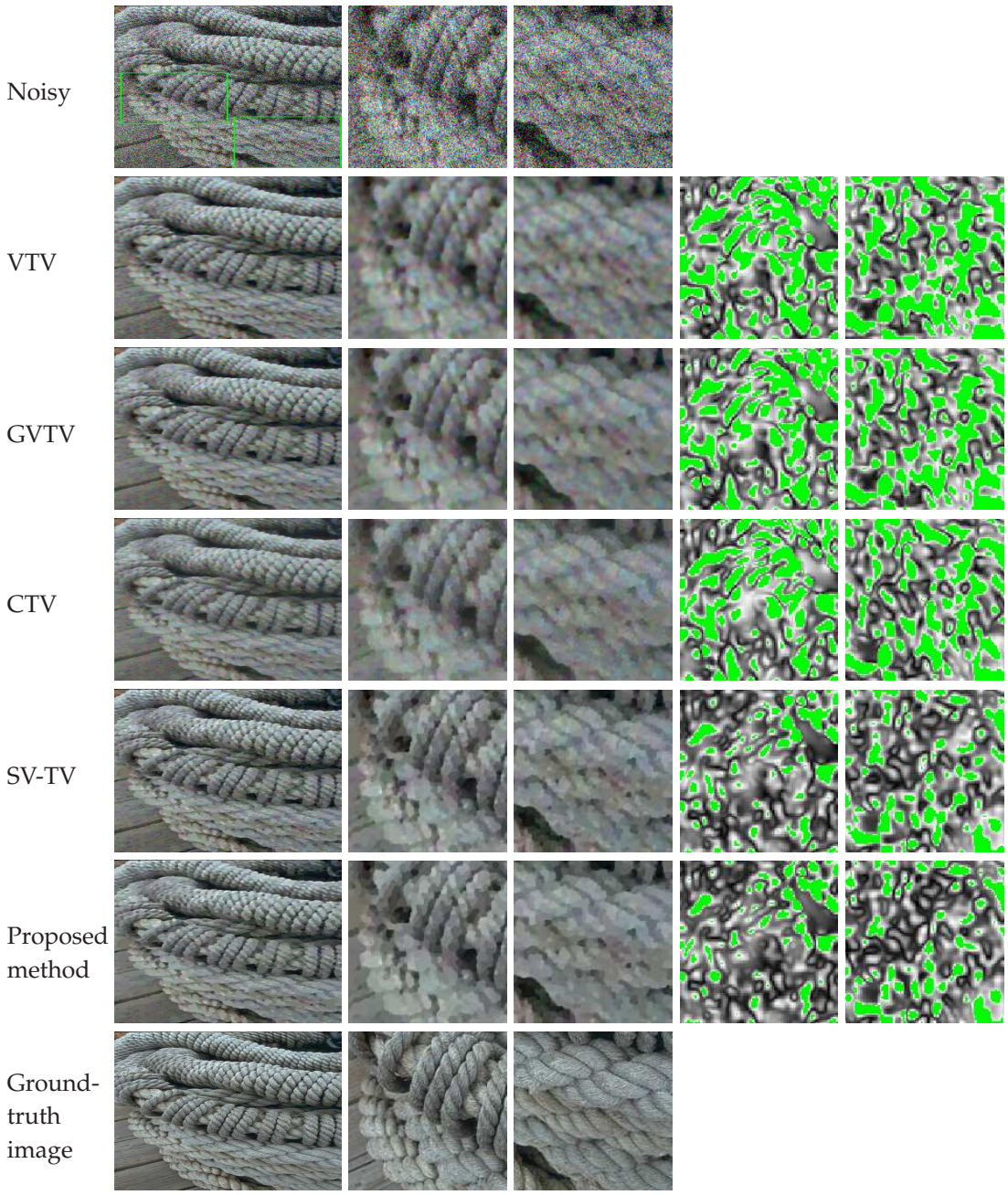

Figure 11: From top to bottom: the noisy image with $\sigma = 0.2$, restored results by using VTV, GVTV, CTV, SV-TV, the proposed method, and the ground-truth image. The corresponding zooming parts are displayed in the second column and the third column. The fourth column and fifth column are the spatial distributions of pixels with S-CIELAB error of the zooming parts.

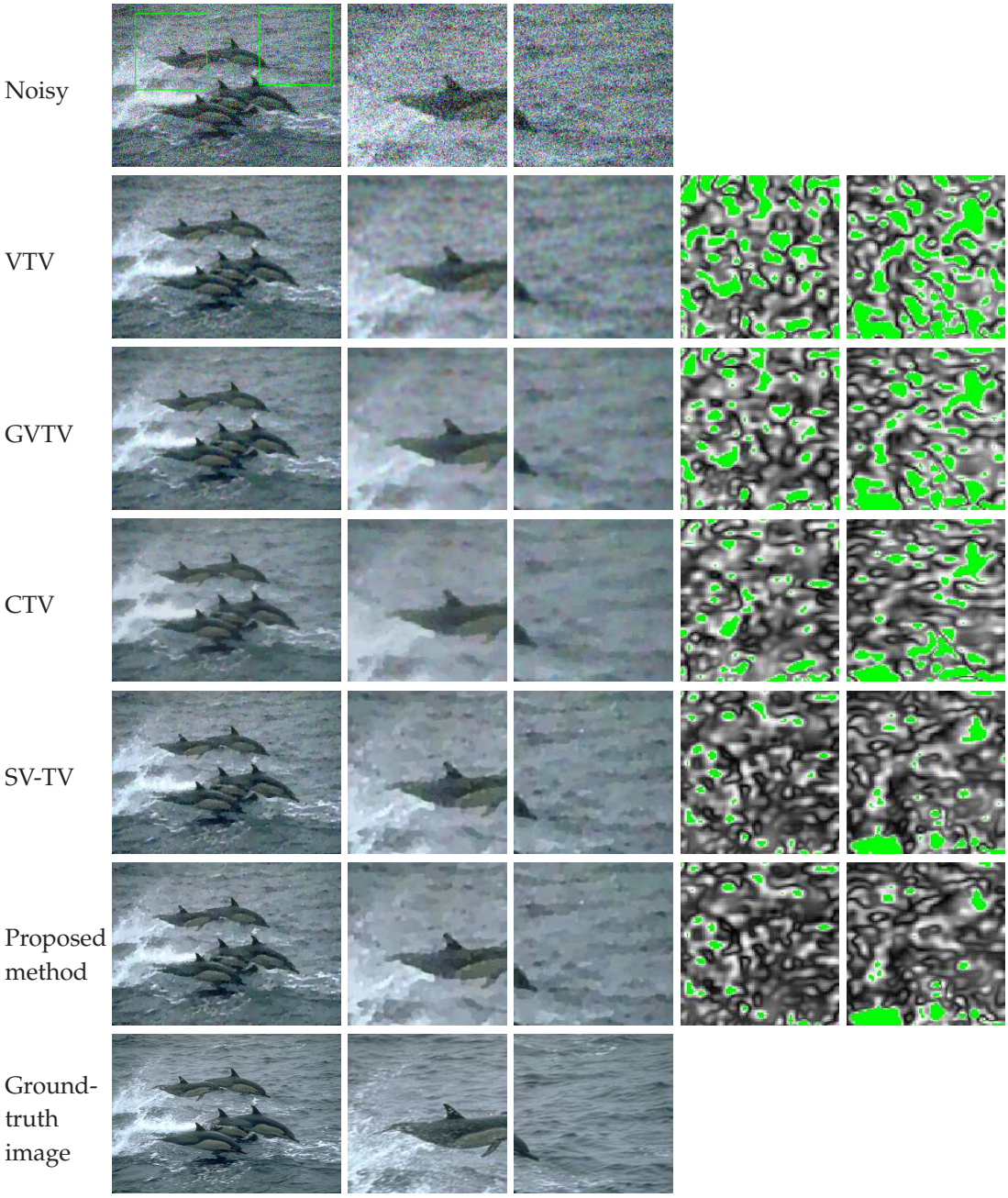

Figure 12: From top to bottom: the noisy image with $\sigma = 0.2$, restored results by using VTV, GVTV, CTV, SV-TV, the proposed method, and the ground-truth image. The corresponding zooming parts are displayed in the second column and the third column. The fourth column and fifth column are the spatial distributions of pixels with S-CIELAB error of the zooming parts.

Table 1: The SSIM, PSNR and S-CIELAB color error values (larger than 5 units) of the restored images by using different methods.

		VTV	GVTV	CTV	SV-TV	Proposed
Fig. 5	SSIM	0.5826	0.5981	0.6312	0.6953	**0.7049**
	PSNR	22.677	22.975	23.544	24.261	**24.310**
	S-CIELAB	38079	35777	28835	18164	**12131**
Fig. 6	SSIM	0.6671	0.4956	0.7120	0.7636	**0.7744**
	PSNR	21.452	21.934	22.296	23.135	**23.236**
	S-CIELAB	43537	37849	32373	21796	**10876**
Fig. 7	SSIM	0.5580	0.5394	0.6761	0.7092	**0.7251**
	PSNR	23.502	24.264	23.790	25.396	**25.418**
	S-CIELAB	32552	28506	25333	17002	**12456**
Fig. 8	SSIM	0.5690	0.3791	0.6187	0.6732	**0.6840**
	PSNR	20.040	20.521	20.814	21.440	**21.533**
	S-CIELAB	80272	71035	65161	48268	**36698**
Average of 20 testing images	SSIM	0.6065	0.6631	0.6735	0.7277	**0.7338**
	PSNR	22.475	23.300	23.035	24.355	**24.444**
	SCIELAB	58356	51222	55447	35788	**29151**

Table 2: The SSIM, PSNR and S-CIELAB color error values (larger than 5 units) of the restored images by using different methods.

		VTV	GVTV	CTV	SV-TV	Proposed
Fig. 10	SSIM	0.6176	**0.6454**	0.6425	0.5323	0.5315
	PSNR	22.826	23.236	22.859	23.755	**23.772**
	S-CIELAB	43958	40157	45859	24906	**20007**
Fig. 11	SSIM	0.5037	0.5234	0.5086	**0.5878**	0.5783
	PSNR	21.948	22.253	22.022	**22.936**	22.892
	S-CIELAB	46754	43019	40205	22270	**17752**
Fig. 12	SSIM	0.6570	0.6912	0.6844	**0.7365**	0.7353
	PSNR	23.756	24.252	23.918	**24.895**	24.844
	S-CIELAB	39193	31408	29840	14773	**12985**
Average of 20 testing images	SSIM	0.5719	0.6256	0.6065	0.6759	**0.6760**
	PSNR	21.973	22.648	21.823	**23.271**	23.263
	SCIELAB	60409	52501	61159	35116	**32239**

6 Concluding remarks

In summary, we propose a novel hue-preserving color image restoration model by using SV-TV. We make use of SV-TV as the regularization term in the proposed functional, and we incorporate an efficient hue-preserving technique into the proposed functional in order to reduce hue loss during regularization. In order to solve the proposed min-

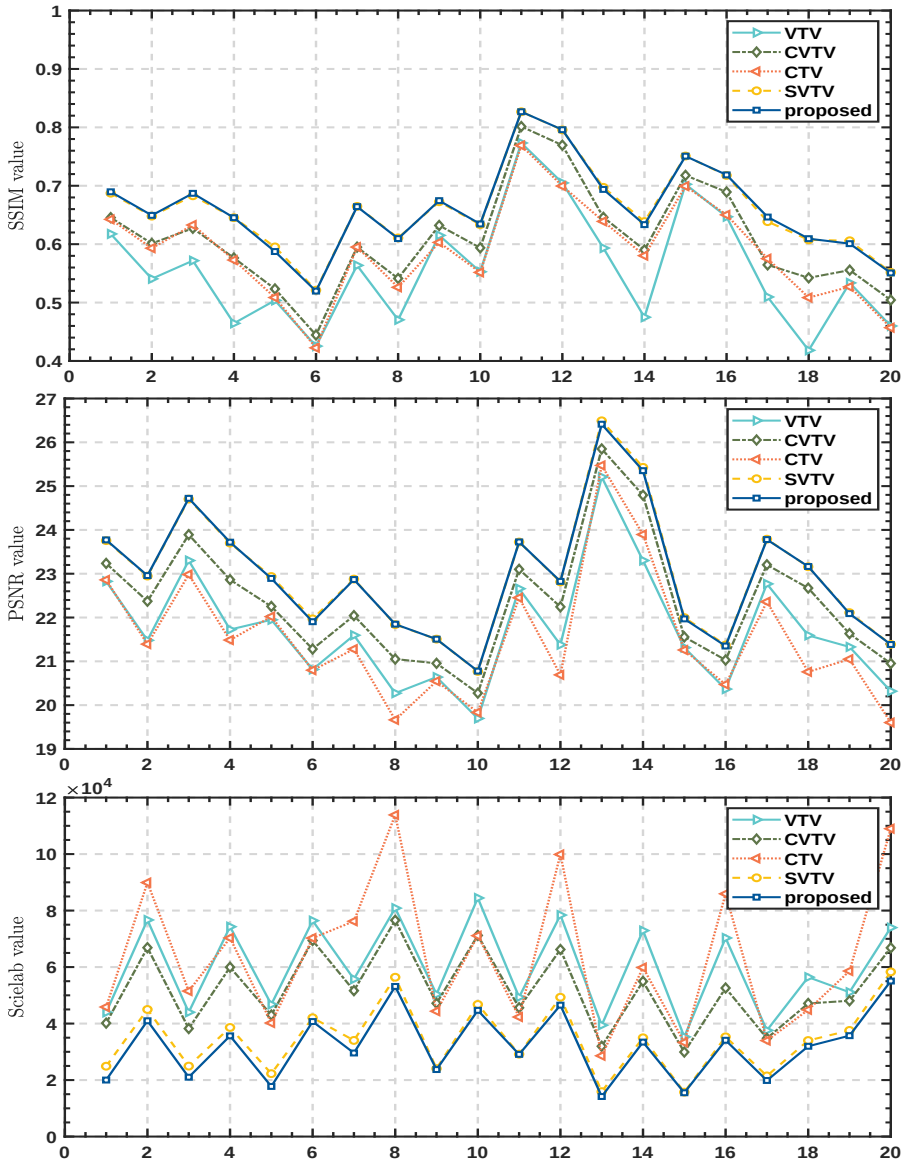

Figure 13: The spatial distributions of SSIM, PSNR and S-CIELAB color error values (between the ground-truth images and the restored results).

imization problem efficiently, we rewrite the proposed model equivalently into a three-block separable convex version. Then we propose a very efficient and effective algorithm with convergence guaranteed to solve the proposed optimization problem. Numerical examples are presented to demonstrate that the performance of the proposed restoration model is better than that of other testing methods in terms of visual quality and some criteria such as peak signal-to-noise ratio, structure similarity, and S-CIELAB color error.

References

[1] T. Azetsu and N. Suetake, *Hue-preserving image enhancement in CIELAB color space considering color gamut*, Opt. Rev., 26:283–294, 2019.

[2] P. Blomgren and T. Chan, *Color TV: Total variation methods for restoration of vector-valued images*, IEEE Trans. Image Process., 7:304–309, 1998.

[3] S. Boyd, N. Parikh, E. Chu, B. Peleato, and J. Eckstein, *Distributed optimization and statistical learning via the alternating direction method of multipliers*, Found. Trends Mach. Learn., 3(1):1–122, 2010.

[4] X. Bresson and T. F. Chan, *Fast dual minimization of the vectorial total variation norm and applications to color image processing*, Inverse Probl. Imaging, 2:455–484, 2008.

[5] J. H. Fitschen, M. Nikolova, F. Pierre, and G. Steidl, *A variational model for color assignment*, in: Scale Space and Variational Methods in Computer Vision. Lecture Notes in Computer Science, Vol. 9087, Springer, 437–448, 2015.

[6] D. Gabay and B. Mercier, *A dual algorithm for the solution of nonlinear variational problems via finite element approximation*, Comput. Math. Appl., 2:17–40, 1976.

[7] R. Glowinski and A. Marrocco, *Sur l'approximation par éléments finis d'ordre un et la résolution par pénalisation-dualité d'une classe de problèmes de Dirichlet non linéaires*, RAIRO Anal. Numer., 2:41–76, 1975.

[8] B. S. He, L. Z. Liao, and M. J. Qian, *Alternating projection based prediction-correction methods for structured variational inequalities*, J. Comput. Math., 24:693–710, 2006.

[9] B. He and X. Yuan, *A class of ADMM-based algorithms for three-block separable convex programming*, Comput. Optim. Appl., 70:791–826, 2018.

[10] X. Ji, *Research on hue-preserving color image enhancement without gamut problem*, in: 2021 IEEE 6th International Conference on Signal and Image Processing, IEEE, 216–222, 2021.

[11] Z. Jia, M. Ng, and W. Wang, *Color image restoration by saturation-value total variation*, SIAM J. Imaging Sci., 12:972–1000, 2019.

[12] D. Martin, C. Fowlkes, D. Tal, and J. Malik, *A database of human segmented natural images and its application to evaluating segmentation algorithms and measuring ecological statistics*, in: Proceedings Eighth IEEE International Conference on Computer Vision ICCV 2001, Vol. 2, IEEE, 416–423, 2001.

[13] D. Menotti, L. Najman, A. de A. Araujo, and J. Facon, *A fast hue-preserving histogram equalization method for color image enhancement using a Bayesian framework*, in: 2007 14th International Workshop on Systems, Signals and Image Processing and 6th EURASIP Conference focused on Speech and Image Processing, Multimedia Communications and Services, IEEE, 414–417, 2007.

[14] S. Naik and C. Murthy, *Hue-preserving color image enhancement without gamut problem*, IEEE Trans. Image Process., 12:1591–1598, 2003.

[15] F. Pierre, J.-F. Aujol, A. Bugeau, G. Steidl, and V.-T. Ta, *Hue-preserving perceptual contrast enhancement*, in: 2016 IEEE International Conference on Image Processing, IEEE, 4067–4071, 2016.

[16] F. Pierre, J.-F. Aujol, A. Bugeau, G. Steidl, and V.-T. Ta, *Variational contrast enhancement of gray-scale and RGB images*, J. Math. Imaging Vision, 57:99–116, 2017.

[17] P. Rodriguez and B. Wohlberg, *A generalized vector-valued total variation algorithm*, in: 2009 16th IEEE International Conference on Image Processing, IEEE, 1309–1312, 2009.

[18] L. I. Rudin, S. Osher, and E. Fatemi, *Nonlinear total variation based noise removal algorithms*, Phys. D, 60:259–268, 1992.

[19] G. Sapiro, *Vector-valued active contours*, in: Proceedings CVPR IEEE Computer Society Conference on Computer Vision and Pattern Recognition, IEEE, 680–685, 1996.
[20] Q.-C. Tian and L. D. Cohen, *Global and local contrast adaptive enhancement for non-uniform illumination color images*, in: 2017 IEEE International Conference on Computer Vision Workshops, IEEE, 3023–3030, 2017.
[21] Z. Wang, A. C. Bovik, H. R. Sheikh, and E. P. Simoncelli, *Image quality assessment: From error visibility to structural similarity*, IEEE Trans. Image Process., 13:600–612, 2004.
[22] C. Yang and J. Rodriguez, *Efficient luminance and saturation processing techniques for bypassing color coordinate transformations*, in: 1995 IEEE International Conference on Systems, Man and Cybernetics. Intelligent Systems for the 21st Century, Vol. 1, IEEE, 667–672, 1995.
[23] X. Zhang and B. A. Wandell, *A spatial extension of cielab for digital color image reproduction*, in: SID International Symposium Digest of Technical Papers, Vol. 27, Citeseer, 731–734, 1996.